Cellular and Molecular Life Sciences (2023) 80:160
https://doi.org/10.1007/s00018-023-04792-x

ORIGINAL ARTICLE

Phosphorylation of STAT3 at Tyr705 contributes to TFEB-mediated autophagy-lysosomal pathway dysfunction and leads to ischemic injury in rats

Yueyang Liu[1] · Xiaohang Che[1] · Xiangnan Yu[1] · Hanxiao Shang[1] · Peirui Cui[1] · Xiaoxiao Fu[1] · Xianda Lu[1] · Yuhuan Liu[1] · Chunfu Wu[1] · Jingyu Yang[1]

Received: 22 January 2023 / Revised: 11 April 2023 / Accepted: 26 April 2023 / Published online: 20 May 2023

Abstract

We previously reported that permanent ischemia induces marked dysfunction of the autophagy-lysosomal pathway (ALP) in rats, which is possibly mediated by the transcription factor EB (TFEB). However, it is still unclear whether signal transducer and activator of transcription 3 (STAT3) is responsible for the TFEB-mediated dysfunction of ALP in ischemic stroke. In the present study, we used AAV-mediated genetic knockdown and pharmacological blockade of p-STAT3 to investigate the role of p-STAT3 in regulating TFEB-mediated ALP dysfunction in rats subjected to permanent middle cerebral occlusion (pMCAO). The results showed that the level of p-STAT3 (Tyr705) in the rat cortex increased at 24 h after pMCAO and subsequently led to lysosomal membrane permeabilization (LMP) and ALP dysfunction. These effects can be alleviated by inhibitors of p-STAT3 (Tyr705) or by STAT3 knockdown. Additionally, STAT3 knockdown significantly increased the nuclear translocation of TFEB and the transcription of TFEB-targeted genes. Notably, TFEB knockdown markedly reversed STAT3 knockdown-mediated improvement in ALP function after pMCAO. This is the first study to show that the contribution of p-STAT3 (Tyr705) to ALP dysfunction may be partly associated with its inhibitory effect on TFEB transcriptional activity, which further leads to ischemic injury in rats.

Keywords Autophagy-lysosomal pathway · Ischemic stroke · Lysosomal membrane permeabilization · Signal transducer and activator of transcription 3 · Transcription factor EB

Introduction

It has been shown that cerebral ischemia is usually associated with autophagy-lysosomal pathway (ALP) dysfunction [1, 2]. Recently, we reported that ALP dysfunction that occurs in rats following permanent middle cerebral artery occlusion (pMCAO) may be due to the loss of lysosome function, mediated by transcription factor EB (TFEB) [3]. However, the mechanisms underlying TFEB-mediated ALP dysfunction after ischemic stroke are not fully understood.

Signal transducer and activator of transcription 3 (STAT3) is a transcription factor that plays a vital role in the regulation of cell growth, cell differentiation, and immune responses [4]. It is well-known that STAT3 transcriptional activity is primarily dependent on the phosphorylation of a single tyrosine (Tyr) residue, Tyr705 [5]. p-STAT3 (Tyr705) can further translocate to the nucleus, and initiate the transcription of its target genes, including a series of autophagy-related genes [6]. However, whether p-STAT3 (Tyr705) exerts an anti- or pro-autophagic effect remains unknown. Over the past few decades, mounting evidence has shown that increased p-STAT3 (Tyr705) level can be observed after ischemic stroke [7] and that its inhibition is beneficial for ischemic outcome [8–10]. Recently, p-STAT3 (Tyr705) has been reported to play an important role in the lysosomal membrane permeabilization (LMP)-mediated cell death during mammary gland involution and breast cancer [11, 12]. Further investigation showed that nuclear STAT3 directly interacts with TFEB, leading to the partial loss of TFEB function, which is essential for lysosomal turnover [13]. However, whether STAT3 is involved in TFEB-mediated ALP dysfunction after ischemic stroke is unknown.

✉ Jingyu Yang
yangjingyu2006@gmail.com

[1] Department of Pharmacology, Shenyang Pharmaceutical University, Shenyang 110016, China

In the present study, we investigated the role of p-STAT3 (Tyr705) in regulating the TFEB-mediated dysfunction of ALP and its contribution to ischemic damage in a rat model of pMCAO. We found that increased p-STAT3 (Tyr705) may contribute to ALP dysfunction in part by inhibiting TFEB transcriptional activity, which further leads to ischemic injury in rats. These results provide insights into the management of ischemic stroke through the development of novel agents targeting STAT3.

Materials and methods

Animals

Male Sprague–Dawley rats weighing 280–320 g (8-week-old) and 150–180 g (4-week-old, for AAV knockdown experiments) were purchased from Changsheng Biotechnology Inco (China), and housed five per cage under standard housing conditions. All animals were adapted to the new environment for 1 week before the experiments were performed. The experiments were conducted and analyzed with a blinded method. All animal experiments complied with the international standards stated in the Guide for the Care and Use of Laboratory Animals, and were approved by the Experimental Animals Ethics Committee of China.

pMCAO model and drug administration

The pMCAO model was conducted as we previously described [14]. Isoflurane was used to anesthetize the animals during the pMCAO procedure. After pMCAO, the rats were warmed on a heating blanket and transferred into their pre-warmed home cage. The animals were sacrificed at the indicated time points by injection of pentobarbital (100 mg/kg) and the brain tissues were harvested. Three criteria were used to ensure successful establishment of the pMCAO model: (1) the ipsilateral cerebral blood flow (CBF) was reduced by more than 70% at 30 min after the arterial occlusion; and (2) the ipsilateral CBF was reduced by more than 50% at 24 h after the arterial occlusion; (3) the modified Neurological Severity Scores (mNSS) > 7 at 24 h (due to subarachnoid hemorrhage) [14]. Total of 350 SD rats were used. Among them, 17 rats died from pMCAO surgery, 35 rats who were not satisfied with above 3 criteria were excluded from the present study. The remaining 298 rats were randomly used for the designed experiments. The STAT3 inhibitors AG490 (S1134), S3I-201 (S1155), and BP-1-102 (S7769) were purchased from Selleck Biotechnology. The three inhibitors were first dissolved in PEG300 and Tween80, and further diluted in normal saline to prepare the working solution before use. AG490 (5 mg/kg) [15, 16] and S3I-201 (5 mg/kg) [17] were administered by intraperitoneal (i.p.) injection at the onset of pMCAO. BP-1-102 (3 mg/kg) [18] was administered by intravenous (i.v.) injection at the onset of pMCAO. Chloroquine (CQ, 60 mg/kg, i.p.; Sigma-Aldrich, C6628) [3] was dissolved in saline and administered at the onset of pMCAO. The Sham or pMCAO rats were injected with an equal volume of solvent.

Measurement of cerebral blood flow

Cerebral blood flow (CBF) was assessed before, at 30 min, and 24 h after pMCAO using the RFLSI Pro laser speckle imaging system (RWD Life Science Co., Ltd). The rats were anesthetized with isoflurane-O_2, and placed in a stereotaxic apparatus in the prone position. The skin was opened to expose the skull. Afterward, the skull was thinned by a high-speed dental drill (STRONG-WT-204) until the blood vessels were clearly visible. The skull was alternately bathed in cold saline to ensure that the brain did not experience damage due to excessive heat during drilling. Laser speckle blood flow images were recorded and CBF was quantified in the same region of interest (ROI) in the right hemisphere.

Measurement of cerebral infarct volume, brain water content, and neurological scores

The rats were sacrificed by decapitation, and their brains were quickly removed, then sliced into five coronal sections at 2-mm intervals. The sections were first incubated with a solution containing 1% 2,3,5-triphenyltetrazolium chloride (TTC; Sigma-Aldrich, T8877) at 37 °C for 20 min, then photographic infarcted areas were taken and further measured using Pro Plus 6.0. The volumes of the infarctions were calculated using the following formula: corrected infarct volume (%) = [contralateral hemisphere volume − (ipsilateral hemisphere volume-infarct volume)]/contralateral hemisphere volume × 100%. The brain water content was determined as an indicator of cerebral edema using a wet/dry method as we previously described. Neurological function was evaluated with the modified Neurological Severity Score (mNSS) test. Each function is graded on a scale of 0–18 (normal score, 0; maximal deficit score, 18). Higher scores indicate more severe behavioral deficits [3].

Immunoblotting

Brain tissues or cells were homogenized in RIPA buffer (Biyotime, P0013B, Nantong, China) containing protease inhibitor cocktail. For solubility fractionation, the tissues were lysed in a lysis buffer containing 1% Triton X-100 (Solarbio, T8200). The lysates were centrifuged to separate the pellets from the supernatants. The pellets were re-suspended in a lysis buffer containing 1% SDS (Solarbio, S8010) and then centrifuged at 12,000×*g* for 15 min. The

supernatants (Triton X-100-soluble fraction) or the re-suspended pellets (Triton X-100-insoluble fraction) were boiled in SDS sample buffer (Solarbio, P1040). An aliquot of 25 μg of total protein from each sample was separated by SDS-PAGE gel electrophoresis, and transferred to a PVDF (Millipore, IPVH00010, Massachusetts, USA) or NC (Pall Life Sciences, 66485, New York, USA) membrane. After blocking with 5% skimmed milk (Becton Dickinson, 232100, New Jersey, USA) at room temperature for 1 h, the membranes were incubated with primary antibodies at 4 °C overnight. The primary antibodies were as follows: anti-ACTB/β-actin (1:1000; Santa Cruz Biotechnology, sc-47778, California, USA), LC3 (1:1000; Medical Biological Laboratories, PM036, Japan), SQSTM1 (1:1000; Abcam, ab56416, Massachusetts, USA), lysosome-associated membrane protein1/LAMP1 (1:1000; Abcam, ab24170), ubiquitin (1:500; Santa Cruz Biotechnology, sc-8017), cathepsin D/CTSD (1:500; Santa Cruz Biotechnology, sc-6487), CTSL (1:1000; R&D Systems, JAI0318071), p-STAT3 (Tyr705) (1:1000; Cell Signaling Technology, 9145), STAT3 (1:1000, Cell Signaling Technology, 9139). After washing three times with TBST, the membranes were then incubated with the secondary antibody (1:5000; ZSGB-BIO, ZB-2301; ZB-2305, Beijing, China) at room temperature for 1 h. The blot was exposed to an ECL blotting system (Thermo Fisher Scientific, 34580, Massachusetts, USA) in accordance with the manufacturer's instructions. The protein levels were quantified by densitometric analysis with ImageJ software (version 2.0, Maryland, USA).

Immunostaining

The animals were perfused with PBS (137 mM NaCl, 2.7 mM KCl, 8 mM Na_2HPO_4, 2 mM KH_2PO_4, pH 7.4, ZSGB-BIO, ZLI-9061) followed by fixed in 4% paraformaldehyde (PFA, Beyotime, P0099, Shanghai, China). Serial coronal brain sections were cut on vibratome (Leica, VT1000S, Wetzlar, Germany) with 40 μm thickness. Antigen was retrieved by incubating with the retrieval solution (ZSGB-BIO, ZLI-9065, Beijing, China) at 85 °C for 30 min. The sections were incubated with 5% PBS-goat serum (ZSGB-BIO, ZLI-9056) containing 0.3% Triton X-100 for 1 h and incubated overnight at 4 °C with primary antibodies against LC3 (1:200; Medical Biological Laboratories, PM036), NeuN (1:500; Millipore, MAB377), LAMP1 (1:200; Abcam, 24170), GFAP (1:400; Abcam, ab4674), Iba1 (1:400; Merck, MABN92), p-STAT3 (Tyr705) (1:100; Cell Signaling Technology, 9145), STAT3 (1:100, Cell Signaling Technology, 9139), and CTSD (1:50; Santa Cruz Biotechnology, sc-6486) overnight at 4 °C. The samples were washed three times in PBS and then incubated for 1 h at room temperature with fluorochrome-coupled secondary antibody (1:200; Alexa Fluor 488, Alexa Fluor 555; Beyotime, A0428; A0516). The nuclei were counterstained with DAPI. Confocal images were acquired using a Nikon Ni-E confocal microscope (Nikon Instruments Inc., Japan) equipped with an A1R scanner (Nikon), 60× objective (Nikon), 130 W metal halide lamp (Nikon), and laser device (Coherent, Coherent Inc., CA, USA). The excitation wavelengths of fluorophores used in this study were 405 nm (50 mW), 488 nm (50 mW), and 561 nm (50 mW). All confocal images were blindly acquired among all groups under the same laser power, pinhole and gain, and were analyzed with Image J (NIH) without adjusting image brightness or contrast.

RNA extraction, reverse transcription, and RT-qPCR

Total RNA was extracted from ipsilateral cortex tissues with TRIzol reagent (Invitrogen) and cDNA was synthetized using FastQuant RT Kit (Tiangen, KR106, Beijing, China). Reverse transcription was performed using oligo (dT) primers. Messenger RNA (mRNA) was quantified using the SYBR green-based RT-qPCR kit (Takara) with the Real Time PCR Detection System (Bio-rad). The primer sequences are shown in Table 1. The PCR conditions were as follows: denaturation at 95 °C for 30 s, followed by 40 cycles

Table 1 Primer sequences

ID	Sense primer (5′–3′)	Antisense primer (5′–3′)
Stat3	CCGGCCCTTAGTCATCAAGAC	CAGGAAATTTGACCAGCAACCT
Tfeb	ACAAGGCACCATCCTCA	CCAGCTCGGCCATATTCA
Map1lc3b	GGAAGATGTCCGGCTCATC	CTTCTCACCCTTGTATCGCTCTA
Sqstm1	CATCTTCCGCATCTACATTAA	TAGCGAGTTCCCACCACA
Lamp1	CCACGTTCAGCACCTCCA	GACCCAAACCTGTCACTTTCTAC
Lamp2	CAGATTCAAAGGGTACTTG	CATTCTTATCATCGCCAC
Ctsb	AGGCTGGACGCAACTTCTAC	ACTGTTCCCGTGCATCAAA
Ctsd	CCTGGGCGATGTCTTTATTG	GGCAAAGCCGACCCTATT
Ctsl	GGCTATGGTTATGAAGGAACA	TTCGGATGTAGTGTCCGTCA
β-actin	GAAGTACCCCATTGAACACGG	TGGGTCATCTTTTCACGCTTG

of 95 °C for 15 s, 60 °C for 45 s. Data were quantified using the $2^{-\Delta\Delta Ct}$ method and normalized to β-actin expression.

Lysosome isolation

The lysosomal fractions from ipsilateral cortex tissues were isolated using a Lysosome Isolation Kit according to the manufacturer's protocol (Sigma-Aldrich, LYSISO1). Briefly, the tissue sample was washed three times with cold PBS, and homogenized at 8000×rpm for 5 s followed by two additional homogenizations at 9500×rpm for 5 s each. The homogenate was centrifuged at 1000×*g* for 10 min at 4 °C, and the pellet was re-suspended with the extraction buffer and re-homogenized at 9500×rpm for 5 s, then centrifuged at 20,000×*g* for 20 min at 4 °C. After the floating fat layer was removed, the pellet was re-suspended with extraction buffer to yield the crude lysosomal fraction (CLF). To further enrich the lysosomes in the CLF, the CLF was diluted by 19% OptiPrep Density Gradient Medium solution with a protein concentration of 10 mg/mL. This solution is called the diluted OptiPrep fraction (DOF). The DOF was separated by density gradient centrifugation (150,000×*g* for 4 h) on a multi-step OptiPrep gradient.

AAV packaging and stereotactic injection

A selected shRNA sequence for rat *Stat3* or a scramble control were inserted into the AAV vector. The final recombinant AAV2/9 expression cassette was ITR-CMV bGlobin-eGFP-WPRE-hGH polyA-U6-shSTAT3-ITR. The *Stat3* shRNA sequence was 5′-GCTGAACAACATGTCATTT-3′. The resultant AAVs were packaged at Obio Technology Company (Shanghai, China) and concentrated in phosphate-buffered saline (PBS; HyClone, sh30256.01). The stereotactic delivery of AAV into the cerebral cortex was performed after the rats (150–180 g) were anesthetized with isoflurane. AAV particles (1 μL) were injected into the cortex at three sites (AP + 1.2 [site 1], 0.3 [site 2], − 0.6 [site 3]; ML + 4; DV − 2 mm from the skull) using a 33G Hamilton syringe with an automatic injector at the rate of 0.25 μL/min [14]. To prevent backflow, the needle was kept in the place for 5 min after the completion of the injection, then withdrawn for a short distance and held in the new position for another 2 min before removal. The rats were allowed to recover for 4 weeks before pMCAO.

Statistical analysis

Graphpad Prism 7.0 software was used to perform the statistical analyses. The data are expressed as mean ± SEM. Differences between two groups were compared with the unpaired *t* test. Differences between three or more groups were compared with one-way or two-way ANOVA followed by the LSD test. Data from the mNSS test were compared using the non-parametric Kruskal–Wallis test. The level of significance was set at $P < 0.05$.

Results

p-STAT3 (Tyr705) is involved in the ischemic injury in rats following pMCAO

We measured CBF in the ipsilateral brain of the rats before, at 30 min, and 24 h after pMCAO using a laser speckle imaging system. As shown in Fig. S1, the CBF in the ipsilateral hemisphere of rats at 30 min and 24 h after pMCAO was reduced by 70–80% and 50–60%, respectively, confirming that all animals in the pMCAO group satisfied the criteria of the pMCAO model. Ischemic stroke can lead to the phosphorylation of STAT3 at Tyr residue 705 [5]. Therefore, we first investigated the expression and localization of p-STAT3 (Tyr705) in the rat cortex following pMCAO. Western blot analysis showed that the level of p-STAT3 (Tyr705) gradually increased and the level of STAT3 gradually decreased from 3 to 24 h after pMCAO compared to that in the sham group ($P < 0.01$, Fig. 1A–C). To identify the subcellular location of p-STAT3 (Tyr705), co-staining of p-STAT3 (Tyr705) with NeuN (neuronal-specific marker), GFAP (an astrocyte-specific marker), and IBA1 (a micro-glial-specific marker) was performed using immunofluorescence. The results showed that within the penumbra regions of the cortex following pMCAO, p-STAT3 (Tyr705) was translocated into the nucleus and co-localized with NeuN, GFAP, and IBA1 ($P < 0.01$, Fig. S2A, B). It has been shown that inhibition of p-STAT3 can exert neuroprotective effects in ischemic stroke [8–10]. Consistent with this, we also found that AG490 (1.25, 2.5, and 5 mg/kg, i.p.), a tyrosine kinase inhibitor that inhibits STAT3 phosphorylation, significantly decreased the brain infarct volume, brain water content, and neurological scores at 24 h after pMCAO in a dose-dependent manner ($P < 0.05$, Fig. 1D–G). These results indicate that pMCAO-induced phosphorylation of STAT3 at Tyr705 may be involved in ischemic injury.

p-STAT3 (Tyr705) contributes to pMCAO-induced LMP in rats

To investigate the role of p-STAT3 (Tyr705) in regulating lysosomal function, we used AG490 and two other p-STAT3 inhibitors, S3I-201 and BP-1-102, which prevented the formation of p-STAT3 (Tyr705) dimers and suppressed the level of p-STAT3 (Tyr705). As shown in Fig. S3A, B, the increased level of p-STAT3 (Tyr705) in the cortex of rats at 24 h after pMCAO was markedly reduced by S3I-201 (5 mg/kg, i.p. $P < 0.05$), BP-1-102 (3 mg/kg, i.v., $P < 0.001$), and

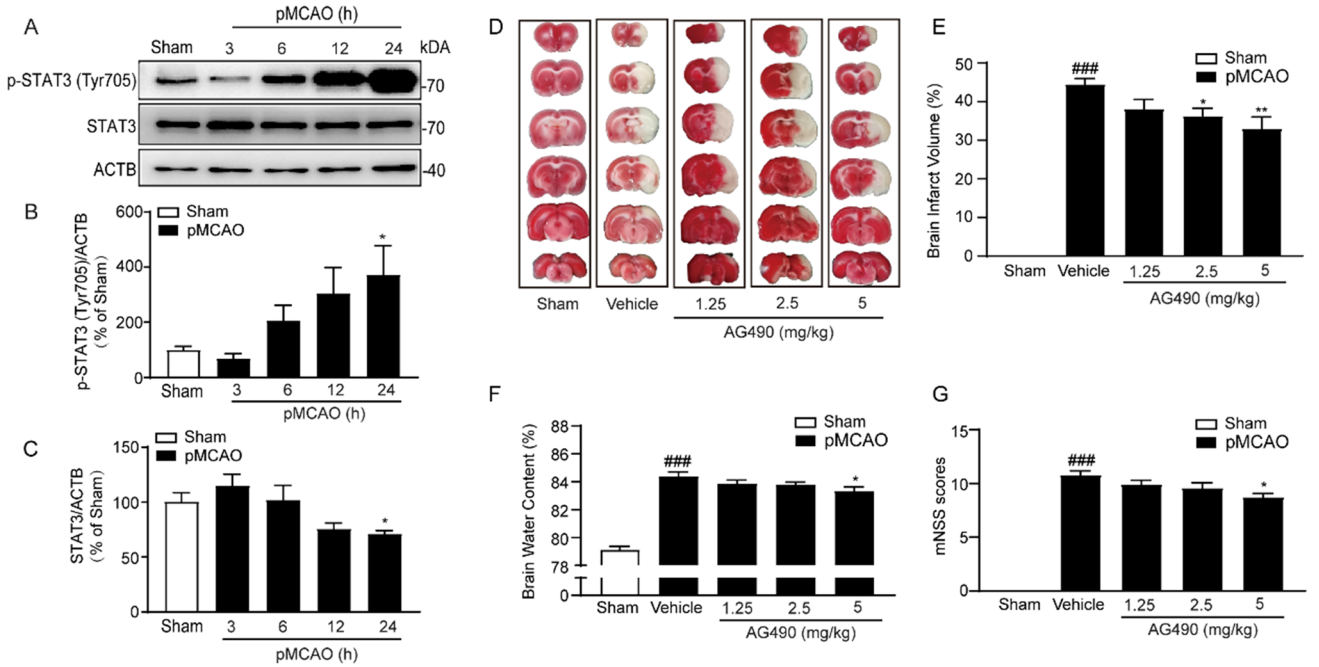

Fig. 1 p-STAT3 (Tyr705) is involved in the ischemic injury in rats following pMCAO. **a** Time-dependent changes of p-STAT3 (Tyr705) and STAT3 levels at 3–24 h in the ischemic cortex of sham- and pMCAO-operated rats. **b**, **c** Quantitative analysis showing the ratios of p-STAT3 (Tyr 705)/ACTB and STAT3/ACTB, measured using Image J software. Statistical comparisons were performed using one-way ANOVA followed by the LSD test. Data are expressed as mean ± SEM from four rats in each group. $^{*}P < 0.05$ vs. sham group. **d** Representative images showing the brain infarct volume of brain slices stained with 2,3,5-triphenyltetrazolium chloride (TTC) in pMCAO rats treated with saline or AG490 (1.25 mg/kg, 2.5 mg/kg, 5 mg/kg, i.p.). Quantification of infarction volume (**e**), brain water content (**f**), and mNSS neurological scores (**g**). Statistical comparisons were performed using one-way ANOVA followed by the LSD test, except for the mNSS neurological scores, which were analyzed using the non-parametric Kruskal–Wallis test followed by Dunn's test. Data are expressed as mean ± S.E.M. from nine to ten rats in each group. $^{###}P < 0.001$ vs. sham group; $^{*}P < 0.05$, $^{**}P < 0.01$ vs. pMCAO group

AG490 (5 mg/kg, i.p., $P < 0.001$) treatment. This confirmed that all three inhibitors significantly decreased the level of p-STAT3 (Tyr705) after pMCAO.

To investigate the role of p-STAT3 (Tyr705) in the regulation of ischemia-induced LMP, the lysosomal and cytosolic fractions were isolated from the cortex of sham- or pMCAO-operated rats. The results showed that the levels of cathepsin D (CTSD) and cathepsin L (CTSL) were reduced in the lysosomal compartment and increased in the cytosolic compartment at 24 h after pMCAO, and these changes were reversed by S3I-201, BP-1-102, and AG490 ($P < 0.05$, Fig. 2A–E). Compared to the vehicle-treated pMCAO group, both BP-1-102 and AG490 reversed the pMCAO-induced decrease in lysosomal membrane-associated protein 1 (LAMP1) ($P < 0.05$, Fig. S4A, B). AG490 reversed the pMCAO-induced decrease in CTSD, and both S3I-201 and AG490 reversed the pMCAO-induced decrease in CTSL ($P < 0.05$, Fig. S4A, C and D).

To further confirm the role of STAT3 in LMP regulation, we generated an AAV delivery system encoding GFP and STAT3 shRNA (sh*Stat3*) to knockdown STAT3 expression (Fig. S3D). After treatment with sh*Stat3*, the levels of STAT3 and p-STAT3 (Tyr705) were significantly reduced in the cortex of sham- and pMCAO-operated rats ($P < 0.05$, Fig. S3E–G), which confirmed that sh*Stat3* specifically targeted and inhibited the expression of endogenous STAT3 and p-STAT3 (Tyr705). Immunofluorescence staining revealed that CTSD mainly co-localized with LAMP1 in GFP-positive cells from sham/sh*Scr* rats, and this co-localization was markedly reduced in the cortex of pMCAO-operated rats, as shown by a lower Mander's coefficient ($P < 0.001$, Fig. 3A, B). STAT3 knockdown significantly restored the co-localization of CTSD with LAMP1 in GFP-positive cells in the cortex of pMCAO/sh*Stat3* rats ($P < 0.001$, Fig. 3A, B). Furthermore, STAT3 knockdown significantly reversed the pMCAO-induced reduction in the level of LAMP1 ($P < 0.05$, Fig. 3C, D) and increased the expression levels of CTSD and CTSL ($P < 0.05$, Fig. 3C, E, F). Overall, these data suggest that the pMCAO-mediated increase of p-STAT3 (Tyr705) contributes to LMP.

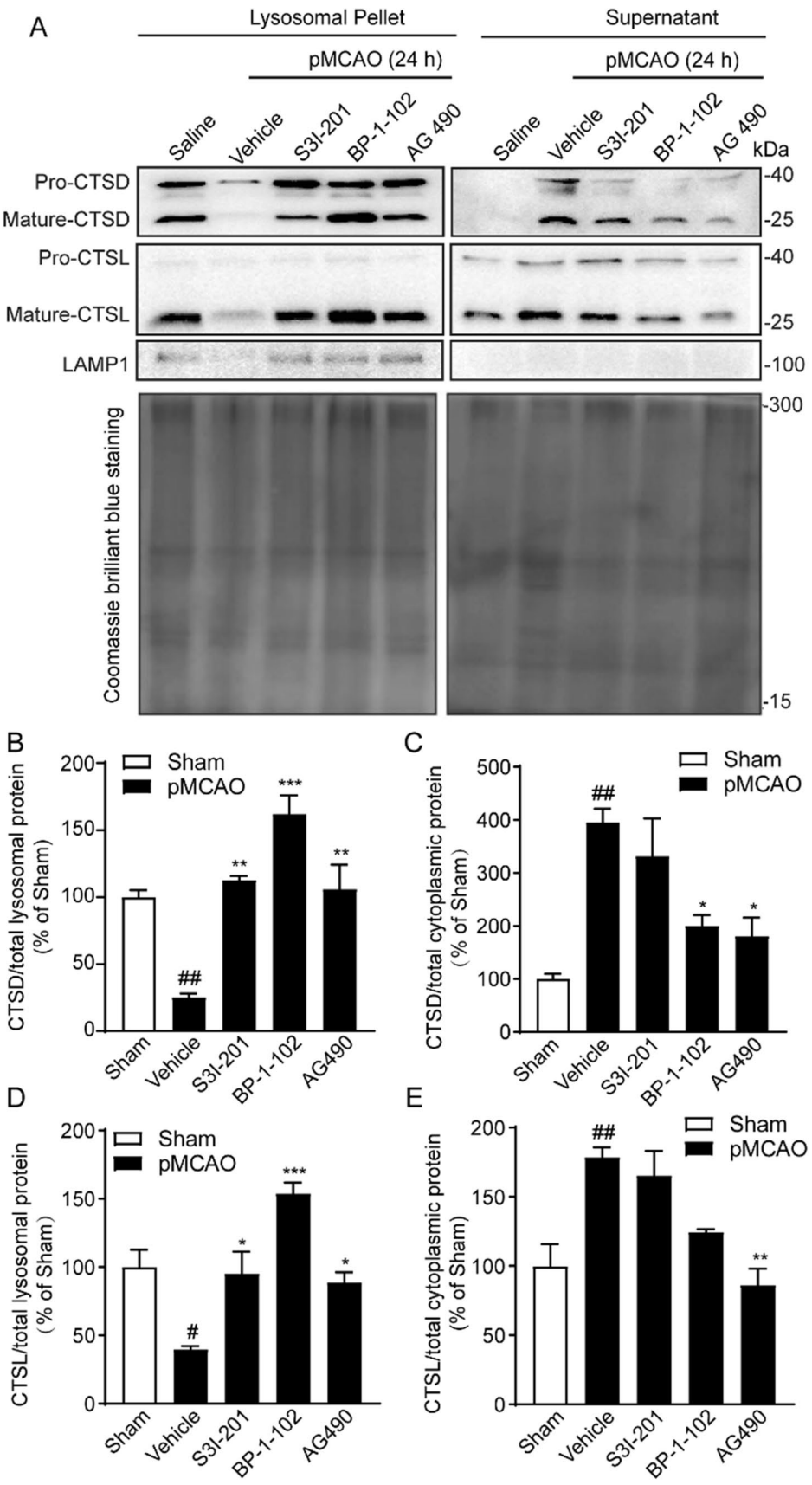

Fig. 2 p-STAT3 (Tyr705) contributes to pMCAO-induced LMP in rats. Rats were treated with three different inhibitors of p-STAT3 (Tyr705), S3I-201 (5 mg/kg, i.p.), BP-1-102 (3 mg/kg, i.v.), and AG490 (5 mg/kg, i.p.), at the onset of pMCAO. **a** Western blot analysis showing the expression levels of CTSD and CTSL in the lysosomal pellet or the supernatant in sham- or pMCAO-operated rats treated with inhibitors of p-STAT3 (Tyr705). Coomassie brilliant blue was used to stain the total protein. Quantitative analysis showing the ratios of CTSD/total lysosomal protein (**b**), CTSD/total cytoplasmic protein (**c**), CTSL/total lysosomal protein (**d**), and CTSL/total cytoplasmic protein (**e**). Statistical comparisons were performed using one-way ANOVA followed by the LSD test. Data are expressed as mean ± SEM from four rats in each group. $^{\#\#}P < 0.01$, $^{\#}P < 0.05$ vs. sham group; $^{***}P < 0.001$, $^{**}P < 0.01$, $^{*}P < 0.05$ vs. vehicle group

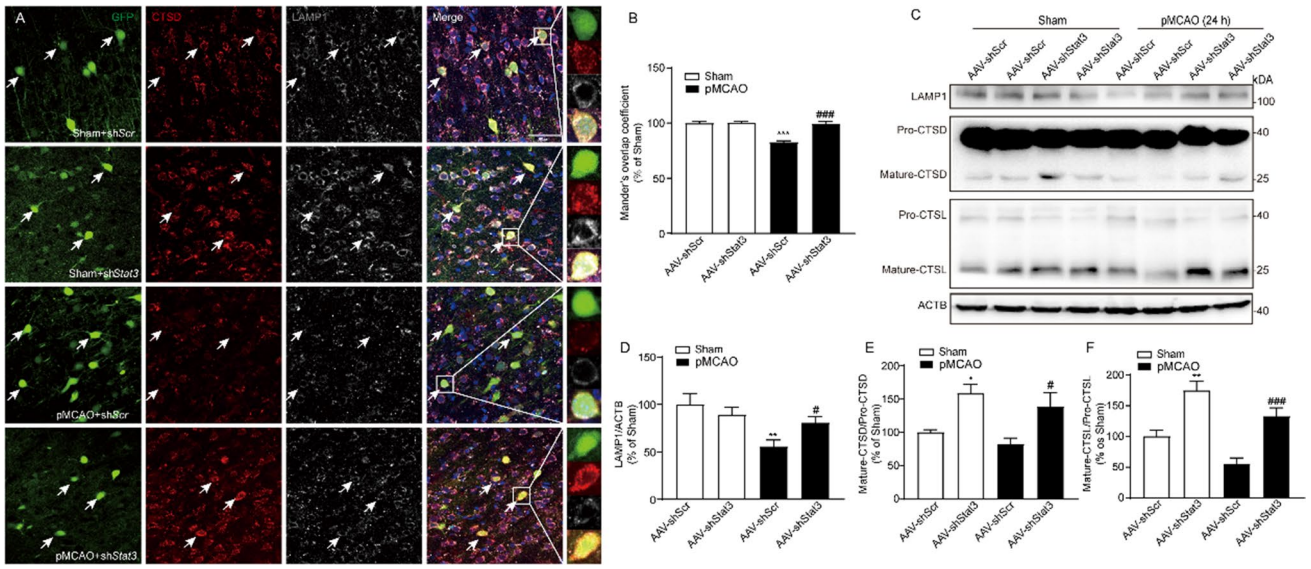

Fig. 3 p-STAT3 (Tyr705) causes lysosomal dysfunction in rats following pMCAO. AAVs encoding GFP and sh*Stat3* or sh*Scramble* (sh*Scr*) were stereotactically injected into the cortex of rats 4 weeks before pMCAO. **a** Rats expressing sh*Stat3* or sh*Scr* were subjected to sham or pMCAO operation. 24 h after surgery, immunofluorescence imaging was performed to detect the co-localization of LAMP1-positive lysosomes (gray) with the lysosomal enzyme CTSD (red) in cells expressing shRNA (indicated by GFP fluorescence, green). Nuclei were stained with DAPI (blue). High-magnification images of the boxed areas are shown at the right. Scale bar = 50 μm. **b** Columns represent Mander's overlap coefficient for CTSD (red) and LAMP1-positive lysosomes (gray). Statistical comparisons were performed using two-way ANOVA followed by the LSD test. Data are expressed as mean ± SEM from four rats in each group. Scale bar = 50 μm. $^{***}P < 0.001$ vs. sham + sh*Scr* group. $^{\#\#\#}P < 0.001$ vs. pMCAO + sh*Scr* group. **c** Western blot analysis showing the expression levels of LAMP1, CTSL, and CTSD in the AAV/shRNA-treated rats at 24 h after sham or pMCAO operation. Quantitative analysis showing the ratios of LAMP1/ACTB (**d**), Mature-CTSD/Pro-CTSD (**e**), and Mature-CTSL/Pro-CTSL (**f**), measured using Image J software. Statistical comparisons were performed using two-way ANOVA followed by the LSD test. Data are expressed as mean ± SEM from four rats in each group. $^{*}P < 0.05$, $^{**}P < 0.01$ vs. sham + shScr group. $^{\#}P < 0.05$, $^{\#\#\#}P < 0.001$ vs. pMCAO + sh*Scr* group

p-STAT3 (Tyr705) causes ALP dysfunction, which further leads to ischemic injury in rats following pMCAO

Next, we determined whether the cerebral ischemia-induced increase of p-STAT3 (Tyr705) influenced ALP function. We investigated the number of autophagosomes and the accumulation of autophagic substrates in pMCAO rats treated with three inhibitors of p-STAT3 (Tyr705). The results showed that the inhibition of p-STAT3 (Tyr705) decreased LC3-II/LC3-I ratio in pMCAO-treated rats ($P < 0.05$, Fig. S5A, B). We examined the levels of two autophagic substrates, SQSTM1 (soluble and insoluble forms) and ubiquitinated proteins. The data showed that the reduced level of soluble SQSTM1 and increased levels of ubiquitinated proteins and insoluble SQSTM1 induced by pMCAO were significantly reversed by STAT3 inhibitors ($P < 0.05$, Fig. S5A, C–E). Fluorescence staining also revealed that LC3 signals were low and diffuse in the cytoplasm of GFP-positive cells in the cortex of sham/sh*Scr* rats, but became punctate and enhanced in the cortex of pMCAO/sh*Scr* rats. Moreover, STAT3 knockdown decreased punctate LC3 fluorescence signals in the GFP-positive cells from both sham- and pMCAO-operated rats ($P < 0.05$, Fig. 4A, B). Western blot analysis also showed that genetic knockdown of sh*Stat3* markedly decreased the accumulation of LC3-II-marked autophagosomes, soluble and insoluble SQSTM1, and ubiquitinated proteins ($P < 0.05$, Fig. 4C–G). Therefore, these results suggest that p-STAT3 (Tyr705) leads to the accumulation of autophagosomes and substrates, contributing to the pMCAO-mediated impairment of ALP function.

To further explore the role of p-STAT3 (Tyr705)-mediated ALP dysfunction in ischemic injury, we investigated the effects of the p-STAT3 inhibitor AG490, combined with the lysosomal inhibitor, chloroquine (CQ, 60 mg/kg, i.p.), on ischemic insult in pMCAO rats. In our previous study, we showed that CQ inhibits autophagic flux [3]. AG490 significantly decreased the infarct volume and brain water content at 24 h after pMCAO, and the effects of AG490 were abolished by CQ ($P < 0.05$, Fig. S6A–C). These results further indicate that p-STAT3 (Tyr705)-mediated impairment of autophagic flux may be responsible for ischemic injury.

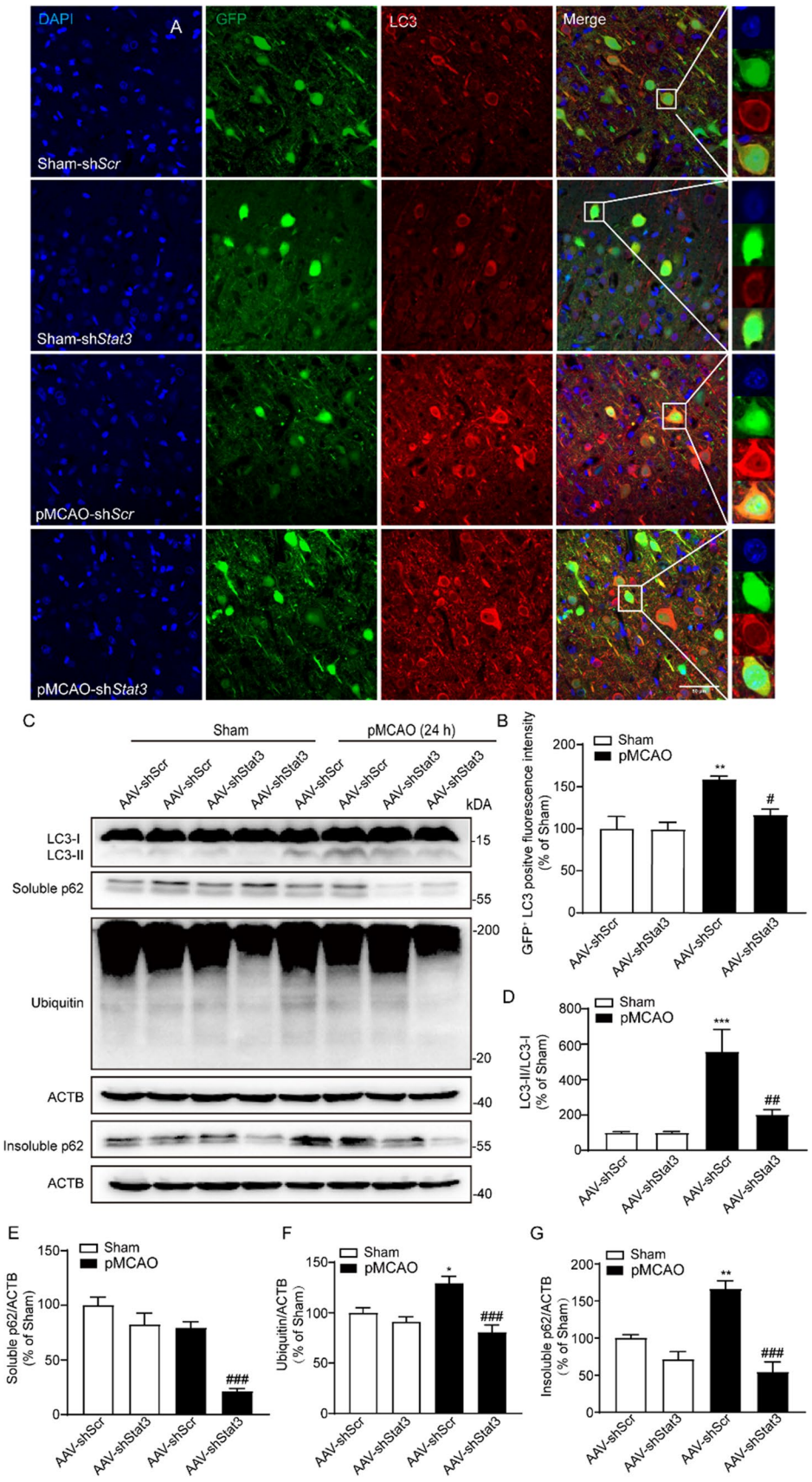

Fig. 4 p-STAT3 (Tyr705) causes dysfunction of ALP in rats following pMCAO. **a** Rats expressing sh*Stat3* or sh*Scr* were subjected to sham or pMCAO operation. 24 h after surgery, immunofluorescence images were captured to detect the expression of LC3 (red) in cells expressing shRNA (indicated by GFP fluorescence, green). Nuclei were stained with DAPI (blue). High-magnification images of the boxed areas are shown at the right. Scale bar = 50 μm. **b** Quantitative analysis showing the fluorescence intensity of GFP^+ LC3, measured using Image J software. Statistical comparisons were performed using two-way ANOVA followed by the LSD test. Data are expressed as mean ± SEM from four rats in each group. $^{**}P < 0.01$ vs. sham + sh*Scr* group. $^{\#}P < 0.05$ vs. pMCAO + sh*Scr* group. **c** Rats expressing sh*Stat3* or sh*Scr* were subjected to sham or pMCAO operation. 24 h after surgery, western blot analysis was performed to analyze the expression levels of LC3-I, LC3-II, soluble SQSTM1, insoluble SQSTM1, and ubiquitin. Quantitative analysis showing the ratios of LC3-II/LC3-I (**d**), soluble SQSTM1/ACTB (**e**), Ubiquitin/ACTB (**f**), and insoluble SQSTM1/ACTB (**g**), measured using Image J software. Statistical comparisons were performed using two-way ANOVA followed by the LSD test. Data are expressed as mean ± SEM from four rats in each group. $^{*}P < 0.05$, $^{**}P < 0.01$, $^{***}P < 0.05$ vs. sham + sh*Scr* group. $^{\#}P < 0.05$, $^{\#\#}P < 0.01$, $^{\#\#\#}P < 0.001$ vs. pMCAO + sh*Scr* group

TFEB may be responsible for p-STAT3 (Tyr705)-mediated ALP dysfunction in rats following pMCAO

As TFEB is vital for maintaining ALP function [19], we investigated whether TFEB is involved in p-STAT3 (Tyr705)-mediated dysfunction of ALP after ischemic stroke. Western blot analysis showed that p-STAT3 (Tyr705) inhibitors significantly increased the expression of TFEB in the total and nuclear extracts of the cortex from pMCAO rats ($P < 0.05$, Fig. 5A–C). Immunofluorescence revealed that STAT3 knockdown enhanced TFEB translocation into the nucleus after pMCAO in rats (Fig. 5D). Furthermore, real-time PCR analysis showed that STAT3 knockdown increased the mRNA levels of the direct target genes of TFEB, including *Ctsd*, *Maplc3b*, *Lamp1*, *Sqstm1*, and *Tfeb*,

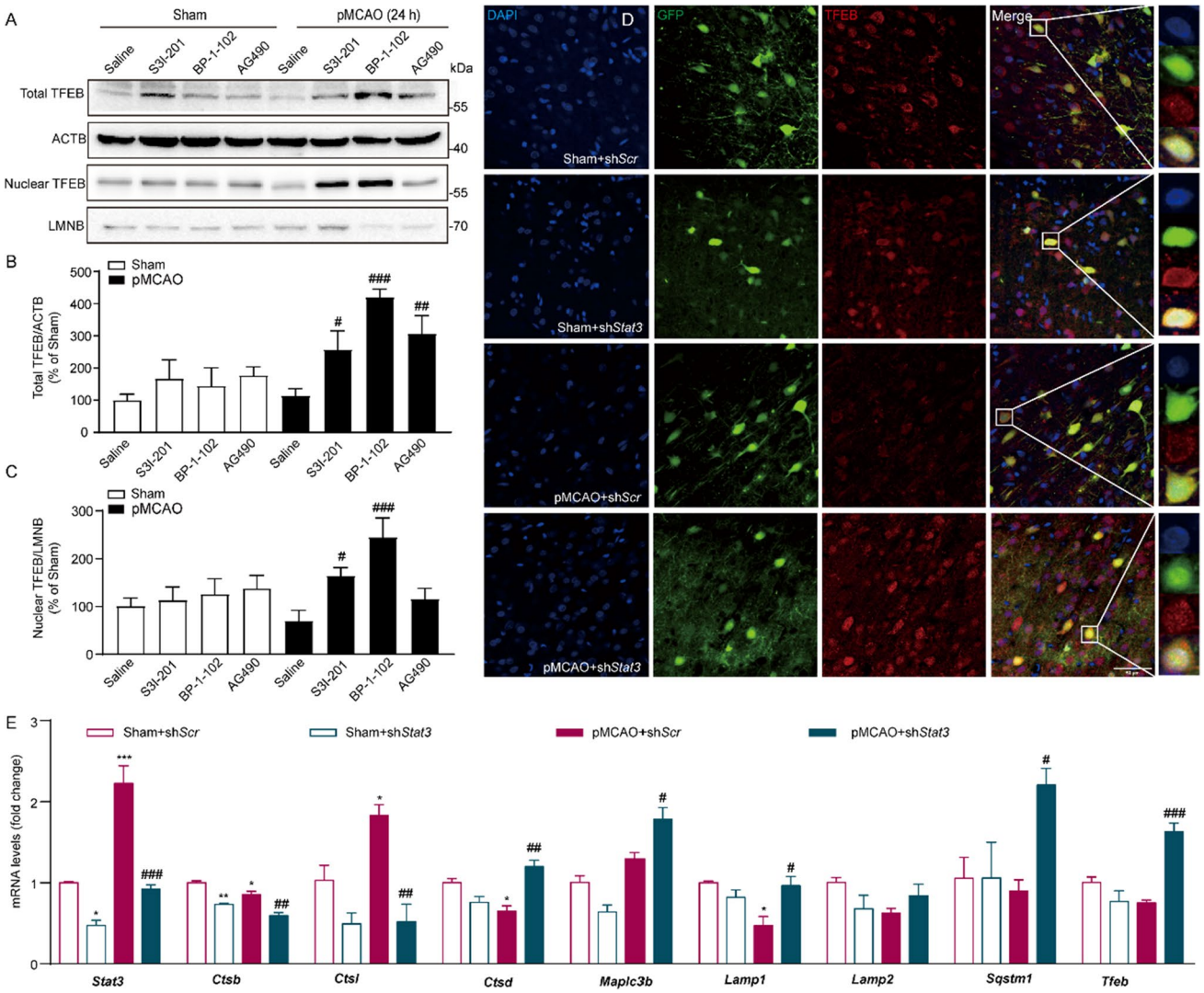

Fig. 5 The pMCAO-mediated increase of p-STAT3 (Tyr705) leads to the inhibition of TFEB transcriptional activity. **a** Western blot analysis showing the expression level of TFEB in total and nuclear protein extracts in sham- or pMCAO-operated rats treated with inhibitors of p-STAT3 (Tyr705). Lamin B (LMNB) was used as a nuclear loading control. Quantitative analysis showing the ratios of TFEB/ACTB (**b**) and TFEB/LMNB (**c**), measured using Image J software. Statistical comparisons were performed using two-way ANOVA followed by the LSD test. Data are expressed as mean ± SEM from four rats in each group. $^{\#}P < 0.05$, $^{\#\#}P < 0.01$, $^{\#\#\#}P < 0.001$ vs. pMCAO group. **d** Rats expressing sh*Stat3* or sh*Scr* were subjected to sham or pMCAO operation. 24 h after surgery, immunofluorescence images were collected to detect the co-localization of TFEB (red) with nuclei (blue) in cells expressing shRNA (indicated by GFP fluorescence, green). High-magnification images of the boxed areas are shown at the right. Scale bar = 50 μm. **e** RT-qPCR analysis showing mRNA expression of *Stat3* and ALP-related marker genes including *Ctsb*, *Ctsl*, *Ctsd*, *Map1lc3b*, *Lamp1*, *Lamp2*, *Sqstm1*, and *Tfeb* at 24 h in the cortex of sham- or pMCAO-operated rats injected with sh*Scr* or sh*Stat3* vectors. Statistical comparisons were performed using two-way ANOVA followed by the LSD test. Data are expressed as mean ± SEM from four rats in each group. $^{***}P < 0.001$, $^{**}P < 0.01$, $^{*}P < 0.05$ vs. sham + sh*Scr* group. $^{\#\#\#}P < 0.001$, $^{\#\#}P < 0.01$, $^{\#}P < 0.05$ vs. pMCAO + sh*Scr* group

but decreased the levels of *Ctsb* and *Ctsl* without influencing the level of *Lamp2* in the cortex of pMCAO rats ($P < 0.05$, Fig. 5E). These data demonstrate that the pMCAO-mediated increase of p-STAT3 (Tyr705) leads to the inhibition of TFEB activity.

Next, we further clarified whether TFEB knockdown could reverse the p-STAT3 (Tyr705)-mediated impairment of ALP function. AAVs encoding sh*Tfeb* and sh*Stat3* were injected into the cortex of rats. Western blot analysis showed that the sh*Stat3*-mediated downregulation of LC3-II and Ubiquitin in the cortex of rats at 24 h after pMCAO was significantly reversed by TFEB knockdown ($P < 0.05$, Fig. 6A–D). These results further indicate that TFEB may be responsible for the p-STAT3 (Tyr705)-mediated dysfunction of ALP after pMCAO.

Discussion

ALP has recently emerged as an attractive target for the treatment of ischemic stroke [2, 14]. Previous studies by us and other researchers have demonstrated that cerebral ischemia can lead to LMP [14, 20, 21], resulting in reduced lysosomal function and subsequent impairment of autophagic flux [14]. Therefore, enhanced lysosomal function may protect against ischemic stroke. In the present study, we found that the increased p-STAT3 (Tyr705) level may contribute to ALP dysfunction, at least in part, through its inhibitory effect on TFEB transcriptional activity, which further leads to ischemic injury in rats (Fig. 7).

It has been shown that ischemic stroke can lead to the increase in the level of p-STAT3 (Tyr705) [8] and p-STAT3

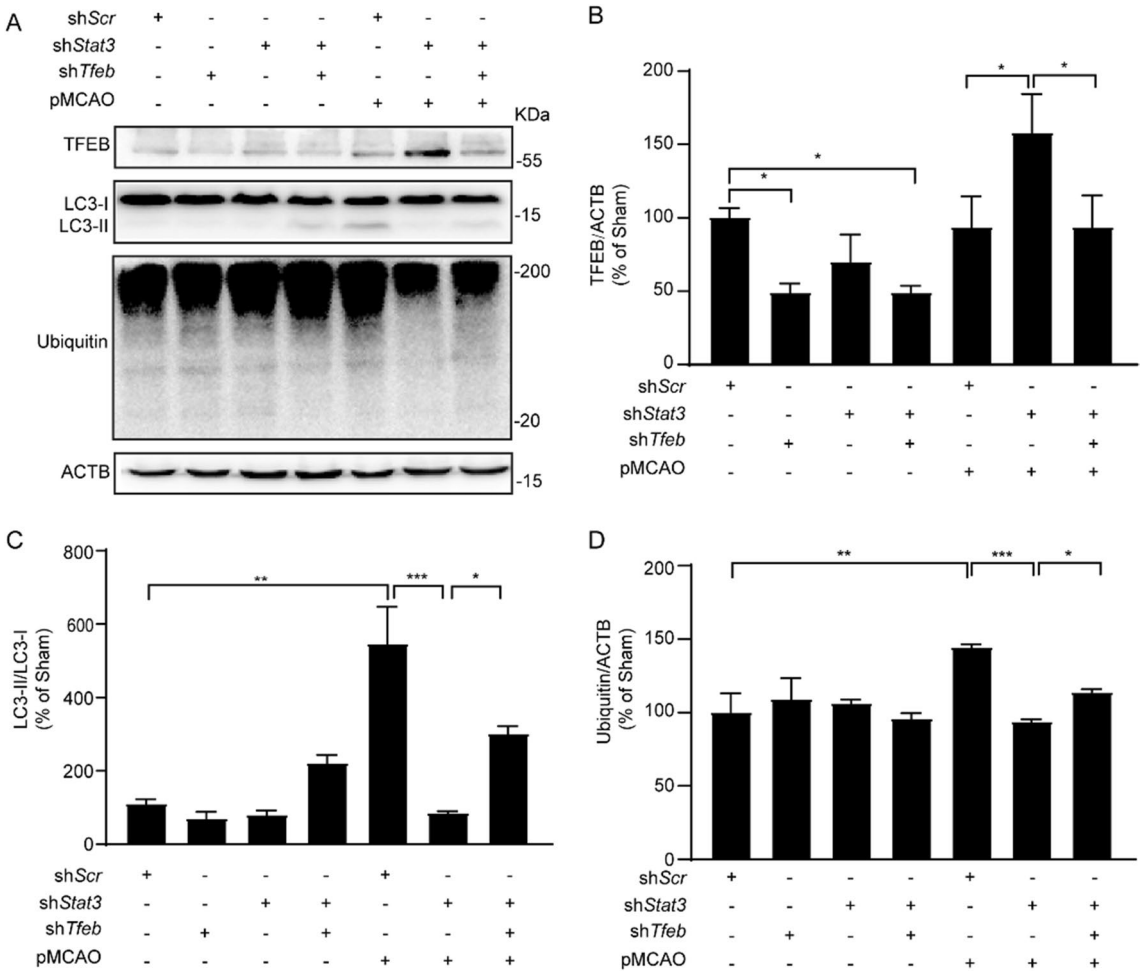

Fig. 6 TFEB may be responsible for p-STAT3 (Tyr705)-mediated dysfunction of ALP after pMCAO. AAVs encoding GFP and sh*Stat3* or sh*Tfeb* were stereotactically injected into the cortex of rats 4 weeks before pMCAO. **a** Western blot analysis showing the levels of TFEB, autophagosomes (LC3-II/LC3-I), and autophagic substrates (Ubiquitin) in the cortex of rats at 24 h after pMCAO. Quantitative analysis showing the ratios of TFEB/ACTB (**b**), LC3-II/LC3-I (**c**), and Ubiquitin/ACTB (**d**), measured using Image J software. Statistical comparisons were performed using one-way ANOVA followed by the LSD test. Data are expressed as mean ± SEM from four rats in each group. $^{*}P < 0.05$, $^{**}P < 0.01$, $^{***}P < 0.001$ vs. the indicated group

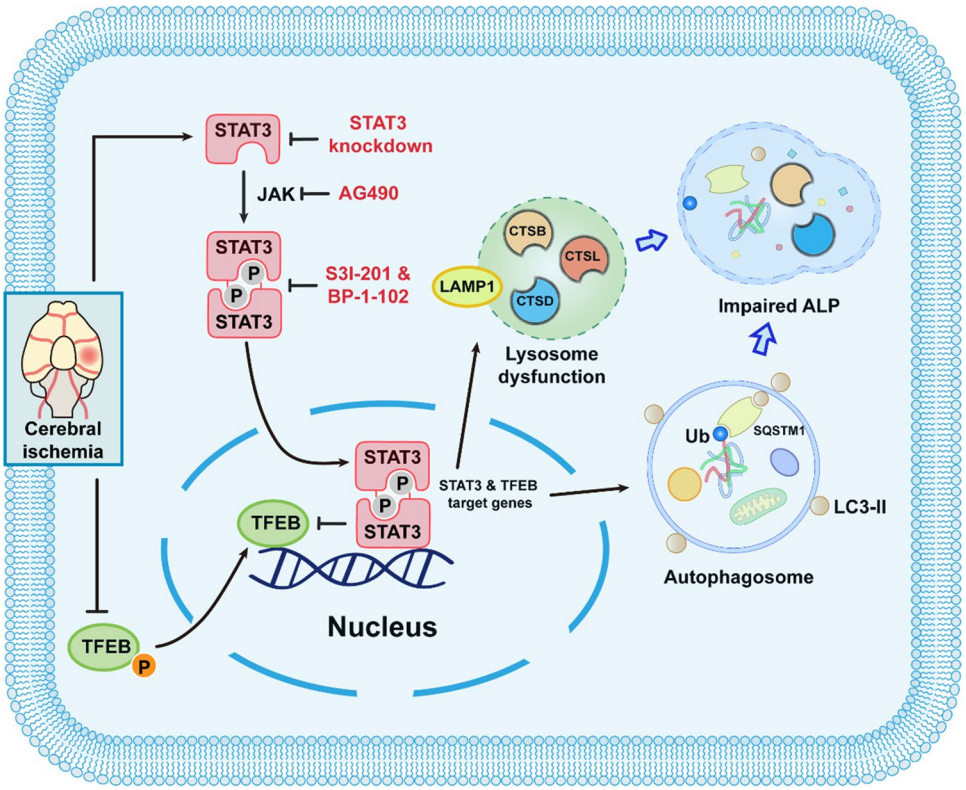

Fig. 7 Schematic representation of the effect of p-STAT3 (Tyr705) on ALP function after ischemic stroke. Permanent ischemic stroke leads to the increase of p-STAT3 (Tyr705), and then translocates into nuclei. The pMCAO-induced nuclear translocation of p-STAT3 (Tyr705) can interact with TFEB and inhibit its transcriptional activity, thus leading to the impairment of ALP function. Moreover, genetic knockdown of STAT3 (using AAV-sh*Sat3*) or pharmacological blockade of p-STAT3 (Tyr705) (using the specific inhibitors AG490, S3I-201 and BP-1-102) significantly decreases the stroke-induced LMP and enhances lysosomal function. This ameliorates the impaired ALP function and accelerates the digestion of autophagic substrates after pMCAO

(Tyr705) inhibitors, especially AG490, have been found to possess anti-ischemic injury effects [8, 22]. Accordingly, in the present study, we found that the level of p-STAT3 (Tyr705) gradually increased after pMCAO, accompanied by increased nuclear translocation of p-STAT3 (Tyr705), and that AG490 was able to alleviate ischemic injury in pMCAO rats. In addition, we also found that the expression of total STAT3 was gradually decreased from 3 to 24 h after pMCAO. However, RT-RCR analysis showed that the mRNA level of *Stat3* was significantly increased after pMCAO. Therefore, we hypothesized that cerebral ischemia may lead to increased degradation of unphosphorylated STAT3. Here, we summarize some possible explanations for these hypotheses. (1) It has been reported that calcineurin promotes the degradation of STAT3 through the ubiquitin–proteasome pathway in hippocampus neurons [23, 24]. Interestingly, both our previous study and studies of other researchers have demonstrated that cerebral ischemia can result in the abnormal activation of calcineurin [3, 25], which may be responsible for the increased degradation of STAT3. (2) It has been shown that hyper-osmolarity can accelerate STAT3 degradation in a proteasome-dependent manner [26]. Cerebral ischemia can lead to hyperosmolar-induced brain edema due to hypoperfusion [27], which maybe another reason for the accelerated degradation of STAT3. In our future research, we will conduct further in-depth studies to test the above hypotheses.

Recently, a transcription-dependent mechanism by which TFEB regulates lysosomal biogenesis and autophagy has been identified [19]. Our previous study demonstrated for the first time that at the later stages of ischemia, a gradual decrease in the level of nuclear TFEB is coupled with a progressive decline in lysosomal activity, accumulation of autophagosomes and autophagy substrates, and ischemic injury [3]. In the present study, we revealed that the inhibition of p-STAT3 (Tyr705) further increased both the total and nuclear expression of TFEB and the expression of TFEB-targeted ALP-related genes. These results indicated that p-STAT3 (Tyr705) interacts with TFEB in the nucleus and inhibits its function, resulting in the impaired autophagic flux at 24 h after pMCAO. To test this hypothesis, we performed simultaneous AAV-mediated knockdown of STAT3 and TFEB and found that knockdown of TFEB partly abolished the effects of sh*Stat3* on ALP function. Similarly, other study has shown that RDD648 facilitates p-STAT3 (Tyr705) translocation into the nucleus and leads to partial loss of TFEB function, resulting in lysosome-mediated cell death and exhibiting potent anticancer activity [13]. Another study showed that the expression and activation of TFEB were enhanced in the early stage of *S. aureus* infection, and then diminished due to the delayed activation of STAT3 [28]. Moreover, it has been shown that trigonochinene E (TE), a natural aromatic tetranorditerpene, can activate protein expression of TFEB and TFEB-mediated lysosomal

biogenesis through downregulation of p-STAT3 (Tyr705) [29]. All these studies demonstrate that nuclear p-STAT3 (Tyr705) can inhibit TFEB function, which is consistent with the results of the present study. However, the exact regulatory mechanism through which p-STAT3 (Tyr705) inhibits TFEB activity remains unknown. Based on current evidence, we hypothesize that two possible mechanisms may be involved in this process, namely (1) As a central transcriptional regulator of autophagy, TFEB can bind to the CLEAR element through the basic helix–loop–helix (bHLH) domain and promote lysosomal biogenesis and function. Interestingly, Chen et al. reported that the elimination of STAT3 expression by STAT3 siRNA significantly upregulated the expression of some bHLH transcription factors [30]. Another study also revealed that the downregulation of p-STAT3 (Tyr705) is accompanied by the upregulation of bHLH transcription factors [31]. These studies indicate that p-STAT3 (Tyr705) may directly bind to the bHLH domain of TFEB and further block the TFEB–CLEAR interaction. Thus, it is reasonable to assume that p-STAT3 (Tyr705) may bind to the bHLH domain of TFEB to clash with DNA recognition and disrupt the TFEB–CLEAR interaction after ischemia, which further inactivate TFEB-targeted genes and its own transcription. (2) It has been shown that another member of the TFEB family, MITF, can be negatively controlled by p-STAT3 (Tyr705). The authors observed that activated p-STAT3 (Tyr705) can downregulate the mRNA and protein expression of MITF by activating the CAAT enhancer binding protein (CEBP), a well-established downstream target of STAT3. Activated CEBP further binds to the MITF enhancer region and silences MITF expression [32]. Because TFEB and MITF share sequence homology, this mechanism may also be involved in the biological processes of p-STAT3 (Tyr705)-mediated TFEB expression. However, these hypotheses require further investigations.

It has been shown that p-STAT3 (Tyr705) can transcriptionally regulate a series of autophagy-related genes [6]. However, whether p-STAT3 (Tyr705) exerts an anti- or pro-autophagic effect remains unknown. STAT3 transcriptionally activates BCL2 and MCL1 expression [33, 34] and directly binds to the promoter region of BECN1 and represses its transcription [35], which leads to autophagy inhibition. In contrast, STAT3 phosphorylation upregulates BNIP3 expression, leading to autophagy induction [36]. In addition to its direct effect on the regulation of autophagy-related proteins, cytoplasmic STAT3 interacts with other transcription factors, such as FOXO1 and FOXO3, thus indirectly regulating autophagy [37]. To comprehensively evaluate the role of p-STAT3 (Tyr705) in the ischemia-induced dysfunction of ALP, we used two other inhibitors of p-STAT3 (Tyr705), S3I-201 and BP-1-102, in addition to AG490. Furthermore, we used an AAV encoding sh*Stat3* to specifically knockdown STAT3 expression. We found that both pharmacological inhibition and gene knockdown of p-STAT3 (Tyr705) alleviated LMP by preventing pMCAO-induced downregulation of LAMP1 and the release of cathepsin proteases from lysosomes into the cytosol. Western blot analysis also showed that protein expressions of CTSL and CTSD were downregulated after ischemic stroke, which were partly reversed through STAT3 inhibition. Notably, *Ctsd* has been identified as a direct target of TFEB [38]; therefore, the STAT3-mediated upregulation of CTSD after ischemic stroke may be attributed to the post-transcriptional regulation of TFEB. Moreover, *Ctsl* has been demonstrated to be a direct target gene of STAT3 [6]; however, the protein level of CTSL was also upregulated after STAT3 inhibition following pMCAO. Although CTSL has not been identified as a direct target of TFEB, the activity of which has been reported to be associated with TFEB function [39, 40]. Accordingly, we conclude that the inhibition of p-STAT3 (Tyr705) expression may post-transcriptionally enhance the protein levels of CTSD and CTSL, which may depend on the regulatory effects of TFEB.

To further confirm the role of p-STAT3 (Tyr705) in the regulation of ALP function, we evaluated the formation of autophagosomes and the degradation of substrates after the inhibition of p-STAT3 (Tyr705) following ischemic stroke. Our results showed that ALP degradation was impaired at 24 h after pMCAO, as indicated by the accumulation of LC3-II/LC3-I and insoluble SQSTM1, which is consistent with our previous studies [3]. Although soluble SQSTM1 was downregulated after pMCAO, this phenomenon may be attributed to the downregulation of the TFEB-induced decrease in the post-transcriptional regulation of SQSTM1, as SQSTM1 is also a well-known TFEB-targeted gene [38]. Moreover, we observed that the inhibition of p-STAT3 (Tyr705) through treatment with its inhibitors significantly downregulated the levels of LC3-II/LC3-I and insoluble SQSTM1, suggesting that impaired ALP function was alleviated by the inhibition of p-STAT3 (Tyr705). However, we found that soluble SQSTM1 was also decreased by the inhibition of p-STAT3 (Tyr705) after pMCAO. Therefore, it is hypothesized that the degradation of SQSTM1 by lysosome induced by the activation of ALP may be the main cause of the decreased level of soluble SQSTM1, but not the upregulation of SQSTM1 induced by TFEB-mediated transcriptional regulation.

The present study demonstrates for the first time that p-STAT3 (Tyr705)-mediated impairment of ALP function significantly aggravates ischemic injury after pMCAO, and that these effects may depend on the regulation of TFEB activity by p-STAT3 (Tyr705). Our study further elucidates the protective effects of STAT3 inhibition against ischemic stroke injury from an autophagy-related perspective.

Supplementary Information The online version contains supplementary material available at https://doi.org/10.1007/s00018-023-04792-x.

Author contributions YL: conceptualization, data curation, formal analysis, investigation, methodology, software, validation, visualization, writing—original draft, writing—review and editing. XC: conceptualization, methodology, software, writing—review and editing. XY: data curation, formal analysis, investigation, methodology, software, validation, visualization. HS: formal analysis, visualization. PC: data curation, formal analysis, investigation, methodology, validation, visualization. XF: validation, visualization. XL: data curation, formal analysis, investigation, methodology. YL: validation, visualization. CW: conceptualization, project administration, resources, supervision, writing—review and editing. JY: conceptualization, project administration, resources, supervision, writing—review and editing.

Funding This project was supported by the National Natural Science Foundation of China (82074056) to Jingyu Yang and by grants from the Natural Science Foundation of Liaoning Province (LJKQZ2021031, 2022-MS-246), and the Science Foundation of Excellent Youth in Shenyang Pharmaceutical University (YQ202108) to Yueyang Liu.

Data availability All data are available in the main text or the supplementary materials.

Declarations

Conflict of interest The authors declare that they have no competing interests.

References

1. Wen YD, Sheng R, Zhang LS et al (2008) Neuronal injury in rat model of permanent focal cerebral ischemia is associated with activation of autophagic and lysosomal pathways. Autophagy 4:762–769. https://doi.org/10.4161/auto.6412
2. Zhang X, Yan H, Yuan Y et al (2013) Cerebral ischemia-reperfusion-induced autophagy protects against neuronal injury by mitochondrial clearance. Autophagy 9:1321–1333. https://doi.org/10.4161/auto.25132
3. Liu Y, Xue X, Zhang H et al (2019) Neuronal-targeted TFEB rescues dysfunction of the autophagy-lysosomal pathway and alleviates ischemic injury in permanent cerebral ischemia. Autophagy 15:493–509. https://doi.org/10.1080/15548627.2018.1531196
4. Miklossy G, Hilliard TS, Turkson J (2013) Therapeutic modulators of STAT signalling for human diseases. Nat Rev Drug Discov 12:611–629. https://doi.org/10.1038/nrd4088
5. Chai EZ, Shanmugam MK, Arfuso F et al (2016) Targeting transcription factor STAT3 for cancer prevention and therapy. Pharmacol Ther 162:86–97. https://doi.org/10.1016/j.pharmthera.2015.10.004
6. You L, Wang Z, Li H et al (2015) The role of STAT3 in autophagy. Autophagy 11:729–739. https://doi.org/10.1080/15548627.2015.1017192
7. Suzuki S, Tanaka K, Nogawa S et al (2001) Phosphorylation of signal transducer and activator of transcription-3 (Stat3) after focal cerebral ischemia in rats. Exp Neurol 170:63–71. https://doi.org/10.1006/exnr.2001.7701
8. Satriotomo I, Bowen KK, Vemuganti R (2006) JAK2 and STAT3 activation contributes to neuronal damage following transient focal cerebral ischemia. J Neurochem 98:1353–1368. https://doi.org/10.1111/j.1471-4159.2006.04051.x
9. Cheng X, Yeung PKK, Zhong K et al (2019) Astrocytic endothelin-1 overexpression promotes neural progenitor cells proliferation and differentiation into astrocytes via the Jak2/Stat3 pathway after stroke. J Neuroinflammation 16:227. https://doi.org/10.1186/s12974-019-1597-y
10. Chen S, Dong Z, Cheng M et al (2017) Homocysteine exaggerates microglia activation and neuroinflammation through microglia localized STAT3 overactivation following ischemic stroke. J Neuroinflammation 14:187. https://doi.org/10.1186/s12974-017-0963-x
11. Kreuzaler PA, Staniszewska AD, Li W et al (2011) Stat3 controls lysosomal-mediated cell death in vivo. Nat Cell Biol 13:303–309. https://doi.org/10.1038/ncb2171
12. Sargeant TJ, Lloyd-Lewis B, Resemann HK et al (2014) Stat3 controls cell death during mammary gland involution by regulating uptake of milk fat globules and lysosomal membrane permeabilization. Nat Cell Biol 16:1057–1068. https://doi.org/10.1038/ncb3043
13. Li L, Sun B, Gao Y et al (2018) STAT3 contributes to lysosomal-mediated cell death in a novel derivative of riccardin D-treated breast cancer cells in association with TFEB. Biochem Pharmacol 150:267–279. https://doi.org/10.1016/j.bcp.2018.02.026
14. Liu Y, Che X, Zhang H et al (2021) CAPN1 (Calpain1)-mediated impairment of autophagic flux contributes to cerebral ischemia-induced neuronal damage. Stroke 52:1809–1821. https://doi.org/10.1161/STROKEAHA.120.032749
15. Dong W, Xian Y, Yuan W et al (2016) Catalpol stimulates VEGF production via the JAK2/STAT3 pathway to improve angiogenesis in rats' stroke model. J Ethnopharmacol 191:169–179. https://doi.org/10.1016/j.jep.2016.06.030
16. Dong Z, Liang X, Zhang Q et al (2021) Folic acid deficiency enhances the Tyr705 and Ser727 phosphorylation of mitochondrial STAT3 in in vivo and in vitro models of ischemic stroke. Transl Stroke Res 12:829–843. https://doi.org/10.1007/s12975-020-00860-7
17. Xu X, Zhi T, Chao H et al (2018) ERK1/2/mTOR/Stat3 pathway-mediated autophagy alleviates traumatic brain injury-induced acute lung injury. Biochim Biophys Acta Mol Basis Dis 1864:1663–1674. https://doi.org/10.1016/j.bbadis.2018.02.011
18. Chen D, Wei L, Liu ZR et al (2018) Pyruvate kinase M2 increases angiogenesis, neurogenesis, and functional recovery mediated by upregulation of STAT3 and focal adhesion kinase activities after ischemic stroke in adult mice. Neurotherapeutics 15:770–784. https://doi.org/10.1007/s13311-018-0635-2
19. Settembre C, Di Malta C, Polito VA et al (2011) TFEB links autophagy to lysosomal biogenesis. Science 332:1429–1433. https://doi.org/10.1126/science.1204592
20. Zhou XY, Luo Y, Zhu YM et al (2017) Inhibition of autophagy blocks cathepsins-tBid-mitochondrial apoptotic signaling pathway via stabilization of lysosomal membrane in ischemic astrocytes. Cell Death Dis 8:e2618. https://doi.org/10.1038/cddis.2017.34
21. Kilinc M, Gursoy-Ozdemir Y, Gurer G et al (2010) Lysosomal rupture, necroapoptotic interactions and potential crosstalk between cysteine proteases in neurons shortly after focal ischemia. Neurobiol Dis 40:293–302. https://doi.org/10.1016/j.nbd.2010.06.003
22. Lei C, Deng J, Wang B et al (2011) Reactive oxygen species scavenger inhibits STAT3 activation after transient focal cerebral ischemia-reperfusion injury in rats. Anesth Analg 113:153–159. https://doi.org/10.1213/ANE.0b013e31821a9fbe
23. Murase S (2013) Signal transducer and activator of transcription 3 (STAT3) degradation by proteasome controls a developmental switch in neurotrophin dependence. J Biol Chem 288:20151–20161. https://doi.org/10.1074/jbc.M113.470583
24. Yang Y, Song S, Min H et al (2016) STAT3 degradation mediated by calcineurin involved in the neurotoxicity of isoflurane.

NeuroReport 27:124–130. https://doi.org/10.1097/WNR.0000000000000509
25. Rosenkranz K, May C, Meier C et al (2012) Proteomic analysis of alterations induced by perinatal hypoxic-ischemic brain injury. J Proteome Res 11:5794–5803. https://doi.org/10.1021/pr3005869
26. Lornejad-Schafer M, Albrecht U, Poppek D et al (2005) Osmotic regulation of STAT3 stability in H4IIE rat hepatoma cells. FEBS Lett 579:5791–5797. https://doi.org/10.1016/j.febslet.2005.09.053
27. Ayata C, Ropper AH (2002) Ischaemic brain oedema. J Clin Neurosci 9:113–124. https://doi.org/10.1054/jocn.2001.1031
28. Rao S, Xu T, Xia Y et al (2020) *Salmonella* and *S. aureus* escape from the clearance of macrophages via controlling TFEB. Front Microbiol 11:573844. https://doi.org/10.3389/fmicb.2020.573844
29. Niu Z, Tang G, Wang X et al (2023) Trigonochinene E promotes lysosomal biogenesis and enhances autophagy via TFEB/TFE3 in human degenerative NP cells against oxidative stress. Phytomedicine 112:154720. https://doi.org/10.1016/j.phymed.2023.154720
30. Chen E, Xu D, Lan X et al (2013) A novel role of the STAT3 pathway in brain inflammation-induced human neural progenitor cell differentiation. Curr Mol Med 13:1474–1484. https://doi.org/10.2174/15665240113139990076
31. Li Y, Zhuang P, Shen B et al (2012) Baicalin promotes neuronal differentiation of neural stem/progenitor cells through modulating p-stat3 and bHLH family protein expression. Brain Res 1429:36–42. https://doi.org/10.1016/j.brainres.2011.10.030
32. Swoboda A, Soukup R, Eckel O et al (2021) STAT3 promotes melanoma metastasis by CEBP-induced repression of the MITF pathway. Oncogene 40:1091–1105. https://doi.org/10.1038/s41388-020-01584-6
33. Feng Y, Ke C, Tang Q et al (2014) Metformin promotes autophagy and apoptosis in esophageal squamous cell carcinoma by down-regulating Stat3 signaling. Cell Death Dis 5:e1088. https://doi.org/10.1038/cddis.2014.59
34. Tai WT, Shiau CW, Chen HL et al (2013) Mcl-1-dependent activation of Beclin 1 mediates autophagic cell death induced by sorafenib and SC-59 in hepatocellular carcinoma cells. Cell Death Dis 4:e485. https://doi.org/10.1038/cddis.2013.18
35. Miao LJ, Huang FX, Sun ZT et al (2014) Stat3 inhibits Beclin 1 expression through recruitment of HDAC3 in nonsmall cell lung cancer cells. Tumour Biol 35:7097–7103. https://doi.org/10.1007/s13277-014-1961-6
36. Pratt J, Annabi B (2014) Induction of autophagy biomarker BNIP3 requires a JAK2/STAT3 and MT1-MMP signaling interplay in Concanavalin-A-activated U87 glioblastoma cells. Cell Signal 26:917–924. https://doi.org/10.1016/j.cellsig.2014.01.012
37. Oh HM, Yu CR, Dambuza I et al (2012) STAT3 protein interacts with Class O Forkhead transcription factors in the cytoplasm and regulates nuclear/cytoplasmic localization of FoxO1 and FoxO3a proteins in CD4(+) T cells. J Biol Chem 287:30436–30443. https://doi.org/10.1074/jbc.M112.359661
38. Palmieri M, Impey S, Kang H et al (2011) Characterization of the CLEAR network reveals an integrated control of cellular clearance pathways. Hum Mol Genet 20:3852–3866. https://doi.org/10.1093/hmg/ddr306
39. Zhang C, Yang H, Pan L et al (2021) Hepatitis B virus X protein (HBx) suppresses transcription factor EB (TFEB) resulting in stabilization of integrin beta 1 (ITGB1) in hepatocellular carcinoma cells. Cancers (Basel) 13(5):1181. https://doi.org/10.3390/cancers13051181
40. Zhao L, Liu X, Xu G et al (2020) Arsenic induces mTOR-dependent autophagy, whereas it impairs the autophagy-lysosome pathway and the potential role of TFEB in cultured dendritic cells. Metallomics 12:1230–1245. https://doi.org/10.1039/d0mt00057d